Current Optics and Photonics
Vol. 5, No. 3, June 2021, pp. 261–269

ISSN: 2508-7266(Print) / ISSN: 2508-7274(Online)
DOI: https://doi.org/10.3807/COPP.2021.5.3.261

Binary-phase Complex Spatial Light Modulators Driven by Mirror Symmetry

Minho Choi and Jaewu Choi*

Department of Information Display, Kyung Hee University, Seoul 02447, Korea

(Received November 24, 2020 : revised March 5, 2021 : accepted March 16, 2021)

Binary-phase complex spatial light modulators (BP-C-SLMs) are proposed and simulated. This study shows that bottom-top mirror-symmetrical uniaxial systems between two orthogonal polarizers allow one to construct BP-C-SLMs. BP-C-SLMs double the information-handling capacity per pixel, compared to the conventional amplitude-only spatial light modulators (A-SLMs), as well as being simply implemented with a single spatial light modulator (SLM), rather than a combination of an A-SLM and a binary-phase SLMs. Under limited conditions, BP-C-SLMs can control only the amplitude in single-phase space, and act as A-SLMs.

Keywords : Bi-phase complex spatial light modulator, Complex spatial light modulator, Liquid-crystal devices, Spatial light modulator
OCIS codes : (090.0090) Holography; (120.5060) Phase modulation; (230.3720) Liquid-crystal devices; (230.6120) Spatial light modulators; (260.5430) Polarization

I. INTRODUCTION

Advanced optical and signal systems require pixelated full-range control of amplitude and phase information of light, with space-independency [1–14]. Devices that manipulate the amplitude or phase information of light in space are referred to as spatial light modulators (SLMs). Typical SLMs control amplitude-only or phase-only information for a specific light polarization, and thus are called amplitude-only spatial light modulators (A-SLMs) and phase-only spatial light modulators (P-SLMs) respectively.

In general, complex light amplitude can be controlled by interconnection or combination of multiple A-SLMs or P-SLMs. The interconnection methods include macro-pixel methods [15–17] and doubly-passed-light systems [18–21]. Macro-pixel (super-pixel) methods employ structured optical sheets (*e.g*. structured half-wave plates, beam splitters, or multiple lenses) to combine 2–4 pixels, which can control phase information [1, 6, 16]. The combined systems can realize full-range complex SLMs (C-SLMs), but require high-resolution optical-sheet manufacturing and alignment technology. This results in reduced spatial resolution [15–17].

The doubly-passed-light systems consist of multiple SLMs or polarizing beam splitters [3, 8, 11, 14]. The multiple SLMs consist of two serially aligned SLMs: one A-SLM, and one P-SLM. Although the structures can encode full-range complex amplitude without losing the spatial resolutions of the employed SLMs, the structures become bulky and require precise alignment [18–21].

In this paper, we propose binary-phase complex spatial light modulators (BP-C-SLMs) with structures that are implementable with almost any uniaxial liquid-crystal modes, such as twisted nematic (TN) or in-plane switching (IPS) modes. The light amplitude can be fully controlled in single-phase space within a certain operating-bias range, and thus this device just acts as an A-SLM. With extension of the operating-bias range, the BP-C-SLM modulates not only the full range of amplitude but also the binary state of phase.

Previously, phase-only SLMs independent of incident polarized light using azimuthally π / 2-rotated bottom-top

*Corresponding author: jaewuchoi@khu.ac.kr, ORCID 0000-0002-4648-9054
Color versions of one or more of the figures in this paper are available online.

geometrical symmetry have been developed [22], whereas this study is the extension of the previous work toward implementing full range C-SLMs. The uniaxial systems having bottom-top mirror symmetry between two polarizers are able to adjust amplitude-only information through the horizontally biased electric field, while the optical phases are limited to binary values (ϕ_A and $\phi_A + \pi$). Under restricted conditions, this BP-C-SLM can only control amplitude information in the single-phase plane (as an A-SLM). Even though the ultimate goal is implementation of C-SLMs without using multiple SLMs, this study is just focused on the implementation of BP-C-SLMs. As a result, the controllable light-information space per pixel becomes doubled, compared to that for an A-SLM, as shown in Fig. 1.

An A-SLM can only control the amplitude of light, as shown in Fig. 1(a), while a BP-SLM can only control its binary phase, as shown in Fig. 1(b). To implement a C-SLM or BP-C-SLM, an A-SLM and a BP-SLM are serially combined, as shown in Fig. 1(c). This study shows that a BP-C-SLM can be implemented by using just a single SLM, as shown in Fig. 1(d).

Figure 1(e) shows how the information doubling is achieved by the BP-C-SLM. As shown from sections (i) to (iv) of Fig. 1(e), the combinations of binary-phase information for the repeated amplitude pattern generate four distinguishable signals, yielding four times the amount of information handled by a simple A-SLM.

BP-C-SLMs can be applied to various areas, such as quantum optics, wave optics, quantum information technology, and digital holograms. For example, unlike a typical display that requires only the adjustment of light intensity, a hologram requires the adjustment of the full complex amplitude of light. As a result, typical A-SLMs or P-SLMs may not be enough to implement a realistic hologram, due to the limited information-handling capacity. Therefore, it is mandatory to improve the information-handling capacity per pixel of SLMs. The lack of information-handling capacity of an SLM causes noise and anti-aliasing effects. One can expect that the BP-C-SLMs shown in this study will show significant improvement in creating holograms, due to the doubling of the information-handling capacity per pixel [23–27].

This study suggests that the BP-C-SLM structure can be extended to realize a full-range C-SLM using just a single pixel, by controlling the polar angular distribution of the liquid-crystal (LC) directors with a vertical electric field. Thus a generalized structure for the BP-C-SLM will play an important role in implementing a full-range C-SLM, in terms of structural simplification, applicability, and scalability.

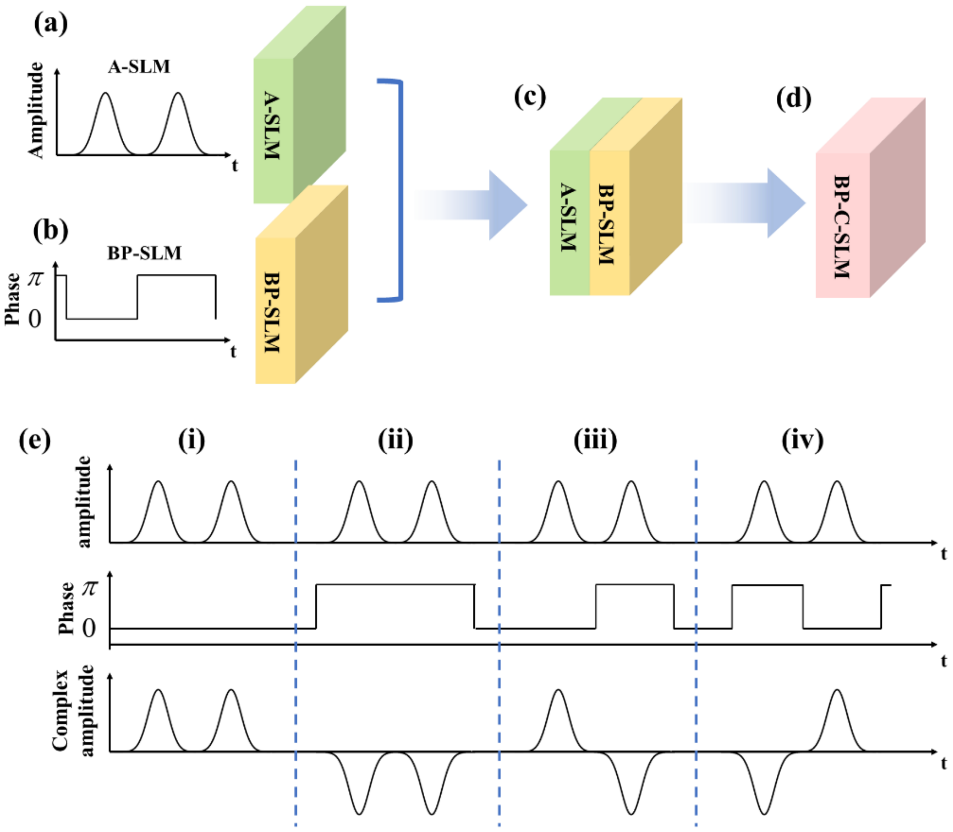

FIG. 1. Schematics of a BP-C-SLM. (a) A-SLM, (b) binary-phase spatial light modulators (BP-SLM), (c) physical combination of one A-SLM with one BP-SLM to achieve a BP-C-SLM, (d) an intrinsically fused BP-C-SLM, and (e) the information-doubling process, using the two physically combined SLMs or the intrinsically fused BP-C-SLM.

Here, for convenience "LC material" represents an anisotropic-birefringence material, and "LC layer" stands for a uniaxial electro-optical anisotropic layer with a specific director direction or wave plates. A specific linear-polarized light field can be written as $\mathbf{E} = E_0 e^{i\delta}$ in phasor form, with the amplitude defined as the positive E_0 and the phase as the angle of the complex value **E** (here, δ of **E**). Thus the complex amplitude of the light field is expressed as amplitude and phase.

II. SINGLE HOMOGENEOUS UNIAXIAL LC LAYER

In this study, light of wavelength λ propagates along the z direction (from bottom to top) through an optical plate located in the xy plane. The optical plate consists of homogeneous LC layers in the xy plane, stacked along the z direction. Thus the specific slow axis or director **n** of each layer varies only with z as $\mathbf{n}(\theta(z), \phi(z))$ where θ and ϕ are the polar and azimuthal angles about the z direction receptively. The uniaxial LC layers have extraordinary and ordinary refractive indices n_e and n_o respectively, and here we assume $n_e > n_o$. The effective refractive indices of each layer with the director of $\mathbf{n}(\theta(z), \phi(z))$ are $n_{o,\text{effective}} = n_o$, $n_{e,\text{effective}} = n_e(\theta) = \{(\cos\theta/n_o)^2 + (\sin\theta/n_e)^2\}^{-0.5}$. $n_e(\theta)$ is just a function of the polar angle θ, and independent of the azimuthal angle ϕ. For any uniaxial system, $n_e(\theta) = n_e(\pi - \theta)$ [28].

Conventionally, the Jones matrix of a homogeneous uniaxial LC layer with thickness d in laboratory coordinates can be expressed by $\mathbf{M}(\theta,\phi,d)$, where the Jones matrix of the uniaxial LC layer in principal coordinates is $\mathbf{W}(\theta,d)$. They are related as below:

$$\begin{aligned}\mathbf{M}(\theta,\phi,d) &= \mathbf{R}(-\phi)\mathbf{W}(\theta,d)\mathbf{R}(\phi) = \mathbf{M}(\phi,\Gamma,\varphi)\\ &= \begin{pmatrix}\cos\phi & -\sin\phi\\ \sin\phi & \cos\phi\end{pmatrix} e^{-i\varphi}\begin{pmatrix}e^{-i\Gamma/2} & 0\\ 0 & e^{+i\Gamma/2}\end{pmatrix}\begin{pmatrix}\cos\phi & \sin\phi\\ -\sin\phi & \cos\phi\end{pmatrix}\\ &= e^{-i\varphi}\begin{bmatrix}e^{-i\Gamma/2}\cos^2\phi + e^{i\Gamma/2}\sin^2\phi & -i\sin(\Gamma/2)\sin 2\phi\\ -i\sin(\Gamma/2)\sin 2\phi & e^{-i\Gamma/2}\sin^2\phi + e^{i\Gamma/2}\cos^2\phi\end{bmatrix},\end{aligned} \quad (1)$$

where the phase retardation Γ and common phase φ can be written as a $\Gamma = (n_e(\theta) - n_o)k_0 d$ and $\varphi = (n_e(\theta) + n_o)k_0 d / 2$ respectively. Here $k_0 = 2\pi / \lambda$, the wave number in free space. $\mathbf{R}(\phi)$ is the rotation matrix of $\mathbf{n}(\theta,\phi)$ from laboratory to principal coordinates.

The off-diagonal components of Eq. (1) consist of only purely imaginary components, while the sign and amplitude can be varied with the phase retardation Γ and azimuthal angle ϕ. By employing two orthogonal polarizers, one can selectively take one of the off-diagonal, purely imaginary components.

In particular, when the polar angle of the wave plate is fixed but the azimuthal angel is varied, the common phase φ is fixed, because it is just a function of polar angle θ, but the amplitude of the off-diagonal components varies with azimuthal angle ϕ. As a result, the common phase is fixed but the amplitude and sign of the off-diagonal component depend on the azimuthal angle ϕ and phase retardation Γ. This allows one to control the amplitude of the light, while its phase can be one of the binary values.

Based on this, one can achieve amplitude modulation with binary phase by mechanically rotating the azimuthal angle of the wave plate for a single pixel, but this may not be applicable to arrays with large numbers of pixels, such as SLMs. However, this can be handily achieved by employing electrically controllable liquid-crystal arrays with a specific requirement of LC layer alignment and modulation, as shown below.

III. ELECTRICALLY CONTROLLABLE BINARY-PHASE COMPLEX SPATIAL LIGHT MODULATOR (BP-C-SLM) WITH MIRROR SYMMETRY

The proposed BP-C-SLM consists of a mirror-symmetrically stacked homogeneous LC layer structure sandwiched between two parallel polarizers with orthogonal transmission axes; the transmission axis of one polarizer $\mathbf{P}(\phi_{\text{arb}})$ is oriented with azimuthal angle ϕ_{arb}, while that of the other $\mathbf{P}(\phi_{\text{arb}} \pm \pi / 2)$ is oriented with $\phi_{\text{arb}} \pm \pi / 2$. For a fixed polar angle of directors, the azimuthal angles of directors and phase retardation of each layer are (bottom-top) mirror-symmetrically distributed with respect to the xy plane at the midpoint of the LC layer structure, as shown in Fig. 2.

One example of a BP-C-SLM is a normally black in-plane switching (NB-IPS)-mode structure with four electrodes, as shown in Fig. 2. The in-plane (horizontal) electric field addressed by the four electrodes (light blue cuboids) controls the director distribution, while it allows for the director distribution to maintain the symmetric conditions (mirror-symmetrically distributed azimuth angle and phase retardation with a fixed polar angle or a fixed polar-angular distribution) during their operations. The right two electrodes are grounded, and the left ones are biased at the same voltage to control horizontally oriented electric fields, as shown in Fig. 2(b). One linear polarizer (purple surface) is aligned to 0° in azimuthal angle at the top surface, and the other linear polarizer (yellow surface) to 90° at the bottom surface respectively. Depending on the electric field strength applied, LC molecules rotate maximally along the field direction, as shown in Figs. 2(d) and 2(e).

Here one can consider the LC cell structure as two parts (bottom and top parts with respect to the xy plane at the middle z point), with each part consisting of n layers. The Jones matrix of each layer for the first-half part (bottom) is expressed by $\mathbf{a}_k$ and each layer of the second-half part (top) is expressed by $\mathbf{b}_k$. The first-half and second-half cell structures can be expressed as matrices **A** and **B** respectively. As a result, each **A** and **B** consists of n LC layers ($\mathbf{a}_k$ and $\mathbf{b}_k$).

The Jones matrix $\mathbf{M}_{\text{a–slm}}$ of the BP-C-SLM consists of the bottom-top symmetrical homogeneous LC layered structure (**A** and **B**) and two polarizers, $\mathbf{P}(\phi_{\text{arb}})$ and $\mathbf{P}(\phi_{\text{arb}} + \pi / 2)$,

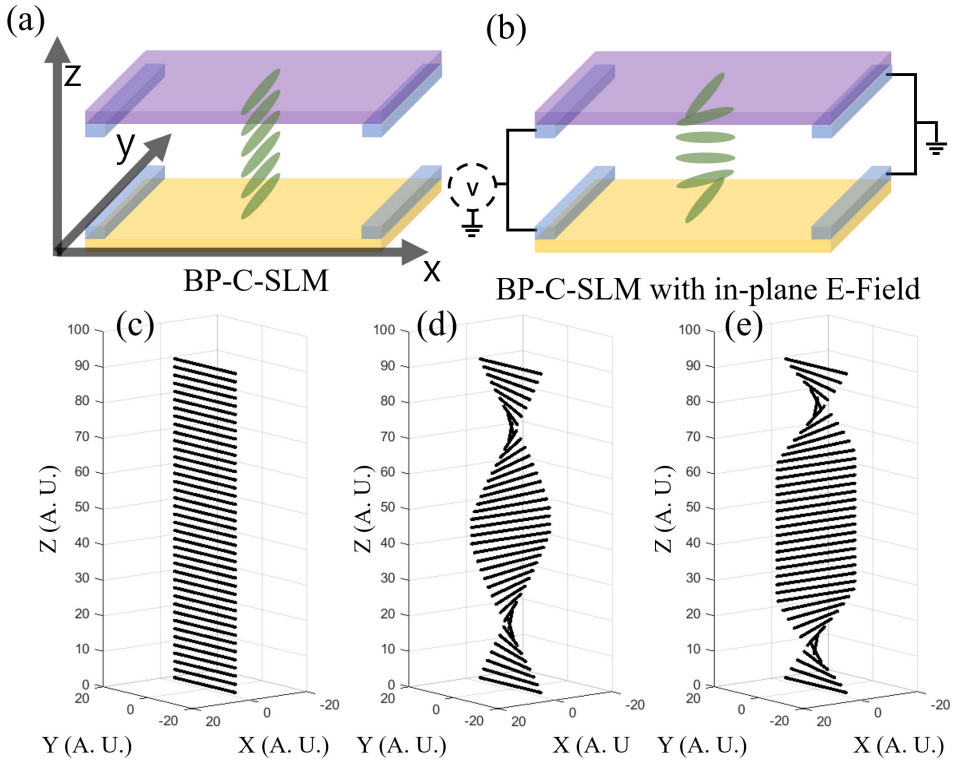

FIG. 2. Schematics of the proposed BP-C-SLMs and their director distributions. (a) and (b) show schematic structures of the proposed BP-C-SLMs based on normally black in-plane switching (NB-IPS) -mode structures, in field off state and on state respectively. The structure consists of four electrodes (blue cuboids), one 0° linear polarizer (yellow surface), and another 90° linear polarizer (purple surface). At the top and bottom surfaces, there are 90° (azimuthal direction) alignment layers of liquid crystal with respect to the *x* axis. (c), (d), and (e) show the director distribution along the *z* direction in the field off and on states respectively. Depending on the strength of applied electric field and *z*, LC molecules rotate toward the applied electric field's direction, as shown in (d) and (e).

with orthogonal transmission axis. The Jones matrix $\mathbf{M}_{\text{a–slm}}$ of the BP-C-SLM can be written as below:

$$\begin{aligned}\mathbf{M}_{\text{a-slm}} &= \mathbf{P}(\phi_{\text{arb}}+\pi/2)\mathbf{B}\mathbf{A}\,\mathbf{P}(\phi_{\text{arb}}) \\ &= \mathbf{P}(\phi_{\text{arb}}+\pi/2)\prod_{k=n}^{1}\mathbf{b}_k(\phi_k,\Gamma_k,\varphi_{\mathbf{B},k})\prod_{k=1}^{n}\mathbf{a}_k(\phi_k,\Gamma_k,\varphi_{\mathbf{A},k})\mathbf{P}(\phi_{\text{arb}}),\end{aligned} \tag{2}$$

where $\mathbf{P}(\phi)=\begin{pmatrix}\cos^2\phi & \cos\phi\sin\phi\\ \cos\phi\sin\phi & \sin^2\phi\end{pmatrix}$.

Let the primed **a'** and **A'** be respectively the Jones matrices of **a** and **A** with zero common phase. Since the common phase components are commutative [Eq. (1)], the Jones matrix for the first-half LC structure can be written as

$$\mathbf{A}=\prod_{k=1}^{n}\mathbf{a}_k(\phi_k,\Gamma_k,\varphi_{\mathbf{A},k})=\prod_{k=1}^{n}\mathbf{a}_k'(\phi_k,\Gamma_k)e^{-i\varphi_{\mathbf{A},k}}=\mathbf{A}'e^{-i\sum_{k=1}^{n}\varphi_{\mathbf{A},k}}. \tag{3}$$

The LC layer structure matrix **A'** can be written in the form of a unitary matrix. Here $\mathbf{A}'=\begin{pmatrix}A & B\\ -B^* & A^*\end{pmatrix}$, where $A=\cos(x)\,e^{ia}$ and $B=\sin(x)\,e^{ib}$. The matrix of the first-half LC structure $\mathbf{A}'=\prod_{k=1}^{n}\mathbf{a}_k'(\phi_k,\Gamma_k)$ without common phases is the transpose of the matrix of the second-half LC structure $\mathbf{B}'=\prod_{k=n}^{1}\mathbf{a}_k'(\phi_k,\Gamma_k)=\prod_{k=1}^{n}\mathbf{b}_k'(\phi_k,\Gamma_k)$, and vice versa [22]:

$$\mathbf{B}'=\mathbf{R}(\pm\pi/2)(\mathbf{A}')^{-1}\mathbf{R}(\mp\pi/2)=(\mathbf{A}')^T. \tag{4}$$

For the cases satisfying two symmetric conditions (the azimuthal angles of directors and phase retardation of each layer have to be mirror symmetrically distributed at a fixed polar angle), a symmetric matrix **SymM** consists of 2*n* LC layers and the symmetric matrix of 2*n* LC layers with zero common phase **SymM'** can be expressed as

$$\begin{aligned}\mathbf{SymM}'=\mathbf{B}'\mathbf{A}'&=(\mathbf{A}')^T\mathbf{A}'=(\mathbf{SymM})\,e^{i\sum_{k=1}^{n}(\varphi_{\mathbf{A},k}+\varphi_{\mathbf{B},k})}\\ &=\begin{pmatrix}A^2+B^{*2} & AB-A^*B^*\\ AB-A^*B^* & A^{*2}+B^2\end{pmatrix}\\ &=\begin{pmatrix}\cos^2(x)\,e^{i2a}+\sin^2(x)\,e^{-i2b} & i\sin(2x)\sin(a+b)\\ i\sin(2x)\sin(a+b) & \cos^2(x)\,e^{-i2a}+\sin^2(x)\,e^{i2b}\end{pmatrix}.\end{aligned} \tag{5}$$

The off-diagonal components of **SymM'** [Eq. (5)] are purely imaginary, as expected. **SymM'**(m, n) is the m^{th} row and n^{th} column component of the **SymM'** matrix. Thus these off-diagonal components of **SymM'** can be expressed as

$$\begin{aligned}&\mathbf{SymM}'(1,2) = \mathbf{SymM}'(2,1)\\&= \mathbf{P}(\pi/2)\mathbf{SymM}'\mathbf{P}(0) = i\sin(2x)\sin(a+b)\cdot\end{aligned} \tag{6}$$

The off-diagonal components of **SymM'** [Eq. (6)] can be selectively taken by the pair of two crossed linear polarizers, as shown in Eq. (6). The off-diagonal terms of **SymM'** show binary phase information ($\pm\pi$ / 2), while the amplitude is modulated and relies on the orientation of the two polarizers with respect to the LC alignment layer and the azimuthal-angle distribution of the **SymM'** structure. Basically, Eq. (6) is of the same form as Eq. (1) because the symmetrical LC layered structure can be reduced to a single wave plate.

From Eq. (6), the output beams can have two different phases of 0 or $\pm\pi$ with respect to each other, because the common phase is fixed for a given polar angle of the director.

If we consider the nonzero common phase of each LC layer to **SymM'**, the total retardation phase is the negative sum of each common average phase of the LC layers plus $\pm\pi$ / 2, as below:

$$\delta_{\text{total}} = \pm\frac{\pi}{2} - \sum_{k=1}^{n}(\varphi_{\mathbf{A},k} + \varphi_{\mathbf{B},k}). \tag{7}$$

The total phase of **SymM** only depends on the polar-angle distribution of LC directors, which determines each common phase of the LC layer. As a result, for a fixed polar-angle distribution, the symmetrical LC structure sandwiched between two orthogonal polarizers allows one to control the amplitude of light at binary phase values.

IV. SIMULATION WITH LINEARLY TWISTED LC LAYERS

4.1. BP-C-SLM structures with linearly twisted LC layers

The modulation properties of the proposed BP-C-SLM structures are investigated by assuming that the rotation of the LC directors is a function of the applied in-plane electric field E_{XY}. The direction of E_{XY} is defined by the azimuthal angle $\phi_{E_{XY}}$ with respect to the entrance polarizer, while its polar angle is fixed at θ = 90°, as shown in Fig. 3. The transmissive axes of the entrance and exit polarizers are the x and y axes respectively, as shown in Fig. 3. Under the in-plane electric field E_{XY}, the azimuthal angles of the LC directors are assumed to vary linearly with z due to the fixed alignment layer, and depend on the strength of the applied electric field before saturation occurred. Saturation of the LC director's rotation is achieved when the azimuthal angle of the LC directors is the same as the azimuthal angle $\phi_{E_{XY}}$ of the applied in-pane electric field. It is assumed that the LC alignment layers have the same direction at the top and bottom surfaces of the LC cell, to satisfy the symmetry requirement. The LC molecules closest to the alignment layers are always aligned parallel to these directions ϕ_{AL}. At zero electric field, all LC directors are directed along ϕ_{AL}. Under an applied electric field, the LC layers in each z position rotate toward the direction of the in-plane electric field $\phi_{E_{XY}}$, but the angle of the rotation depends on z due to the alignment layer. Each LC molecule cannot be rotated more than $\phi_{E_{XY}}$. The maximally twistable angle or saturation angle $\phi_{\text{sat}} = \phi_{E_{XY}} - \phi_{\text{AL}}$ can vary depending on the structure, but in this simulation the saturation angle is chosen to be 90°.

For linearly x-polarized input light with Jones vector $(1,0)^T$, the complex amplitudes of the output y-polarization components $(0,a + bi)^T$ are simulated using the Jones-matrix method and MATLAB R2020b (MathWorks, MA, USA).

Based on this, the azimuthal-angular distribution of the LC directors is assumed to be dependent only on E_{XY} and z. The BP-C-SLM consists of infinitely thin homogeneous LC layers. The azimuthal angle $\phi(z, E_{XY})$ of each LC layer director is linearly varied with $\delta\phi(E_{XY})$ (in degrees/nm) and saturated at $\phi_{E_{XY}}$, as below:

$$\phi(\mathrm{z}, E_{XY}) = \begin{cases} z\delta\phi(E_{XY}) + \phi_{AL} & \text{if } z \le \dfrac{D}{2} \text{ and } z\delta\phi(E_{XY}) + \phi_{AL} < \phi_{E_{XY}} \\ \phi_{E_{XY}} & \text{if } z \le \dfrac{D}{2} \text{ and } z\delta\phi(E_{XY}) + \phi_{AL} \ge \phi_{E_{XY}} \\ \phi_{E_{XY}} & \text{if } z > \dfrac{D}{2} \text{ and } z\delta\phi(E_{XY}) + \phi_{AL} \ge \phi_{E_{XY}} \\ (D - \mathrm{z})\delta\phi(E_{XY}) + \phi_{AL} & \text{if } z > \dfrac{D}{2} \text{ and } z\delta\phi(E_{XY}) + \phi_{AL} < \phi_{E_{XY}} \end{cases}. \tag{8}$$

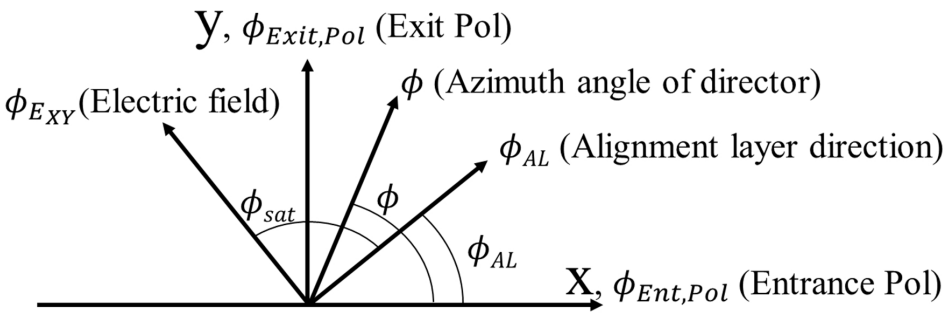

FIG. 3. Directions and angles of LC directors $\mathbf{n}(\theta(z),\phi(z))$, electric field E_{XY} and polarizers **P**.

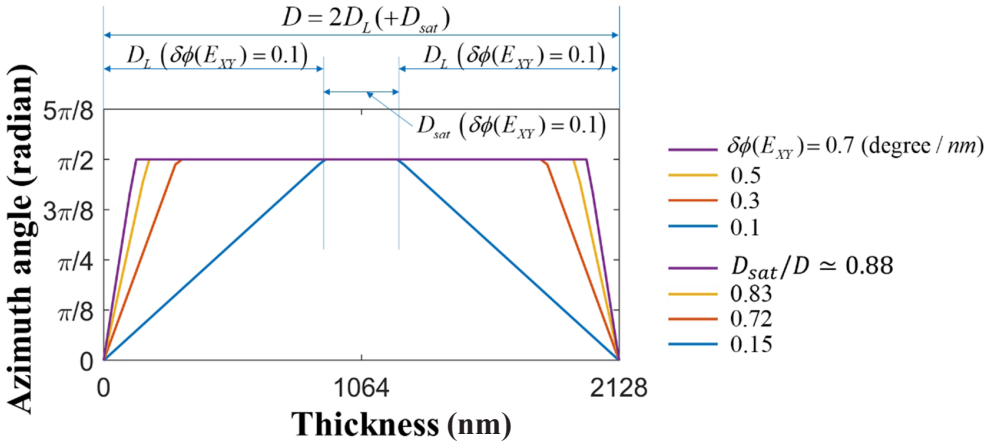

FIG. 4. Azimuthal-angle distributions of LC directors along z (thickness direction) are plotted for $\delta\phi(E_{XY})$ = 0.1, 0.3, 0.5, and 0.7 degrees/nm and $\phi_{AL} = 0°$. The cell thickness is 2128 nm.

A few examples of the azimuthal-angle distributions along the z direction (or LC stacking order) are shown in Fig. 4, when $\delta\phi(E_{XY})$ = 0.1, 0.3, 0.5, and 0.7 degrees/nm, $\phi_{AL} = 0°$, and the total LC cell thickness is 2128 nm. The polar angles θ are fixed at 90°.

The LC cell ($\mathbf{K} = \mathbf{L}^T\mathbf{(WP)L}$) consists of three regions: the linearly positively (negatively) twisted azimuthal-angle region **L**, the wave-plate region **WP** with a constant azimuthal angle of $\phi_{E_{XY}}$, and the linearly negatively (positively) twisted azimuth region $\mathbf{L}^T$. The total cell thickness D can be expressed as the sum of the layer thickness, with two linearly rotated directors in opposite directions (bottom D_L and top D_L) and the saturated layer thickness D_{sat} as marked for $\delta\phi(E_{XY})$ = 0.1 degrees/nm, as shown in Fig. 4. The linearly twisted LC layer can be expressed with Chebyshev's identity [28]. Let $\Gamma(= k_0\Delta nD)$ be the phase retardation in the untwisted state. Let Φ and Γ_L be the maximum twisted angle and phase retardation of region **L** respectively. Γ_{WP} is the phase retardation of the **WP** region D_{sat}. The BP-C-SLM with linear azimuthal-angle variation of the directors can be expressed using Chebyshev's identity $\mathbf{M}^{\text{linear}}_{\text{a-slm}}$, as shown in Eq. (9).

$$\mathbf{M}^{linear}_{a-slm} = \mathbf{P}(\pi/2)\mathbf{KP}(0) = \mathbf{P}(\pi/2)\mathbf{L}^T\mathbf{(WP)LP}(0)$$
$$= \begin{pmatrix} 0 & 0 \\ i2\Phi\dfrac{\sin X}{X}\left(\cos(\Gamma_{WP}/2)\dfrac{\Gamma_L}{2}\dfrac{\sin X}{X} + \sin(\Gamma_{WP}/2)\cos X\right) & 0 \end{pmatrix}, \quad (9a)$$

where

$$X = \sqrt{\Phi^2 + \left(\frac{\Gamma_L}{2}\right)^2},\ \Gamma_{total} = 2\Gamma_L + \Gamma_{WP},\ \Gamma_L = k_0\Delta nD_L,\ \delta\phi = \frac{\Phi}{D_L}. \quad (9b)$$

When $\delta\phi(E_{XY})$ is low or the applied bias voltage is low, the constant wave-plate region may not exist, because there is no saturation. If the saturation exists at a high bias voltage, the saturated ϕ of the directors is equal to ϕ_{sat}.

4.2. Simulation of BP-C-SLM

For the simulations, we assume that the ordinary and extraordinary refractive indices are 1.2 and 1.7 respectively. Here all LC directors are in the xy plane (θ = 90°). The wavelength of the incident light is 532 nm.

The amplitudes and phases of the transmitted light are simulated for two representative configurations of the BP-C-SLM, for thickness of D = 1224, 2232, and 4360 nm for the azimuthal angle of the alignment layer $\phi_{AL} = 0°$, and D = 600, 1680, and 2732 nm for $\phi_{AL} = 45°$.

The transmission amplitude and phase of the transmission coefficient are mapped as functions of $\delta\phi(E_{XY})$ (in degrees/nm), or equivalently as functions of applied in-plane electric field, for the BP-C-SLM with thickness of D = 1224, 2232, and 4360 nm, and azimuthal angle of the alignment layer $\phi_{AL} = 0°$, as shown in Fig. 5.

In this configuration and at $\delta\phi(E_{XY}) = 0$ (in degrees/nm), all LC directors are aligned to $\phi_{AL} = 0°$, which is parallel to the entrance polarizer but orthogonal to the exit polarizer. Thus, this configuration of Fig. 5 secures normally black operation, which is independent of the thickness of the BP-C-SLM.

As $\delta\phi(E_{XY})$ increases, or equivalently the applied bias voltage increases, the amplitude of the transmission coefficient increases, reaches a maximum, and then decreases to zero amplitude (red curves), while the relative phase of the transmission coefficient is constant at 0 (blue lines) and saturation of the LC director rotation is not observed (green curves), as shown in Fig. 5. Again, the amplitude of the transmission coefficient increases as $\delta\phi(E_{XY})$ increases, but the phase of the transmission coefficient (blue lines) jumps to a constant π = 180° while the portion of the saturation region increases (green curves), also as shown in Fig. 5.

These modulation behaviors are repeated more for thicker cells, as seen in Fig. 5. Thus there are alternating regions of constant phase 0 or 180°, while the amplitude of the transmission coefficient increases or decreases as $\delta\phi(E_{XY})$ is varied, or the applied electric field is controlled. This shows

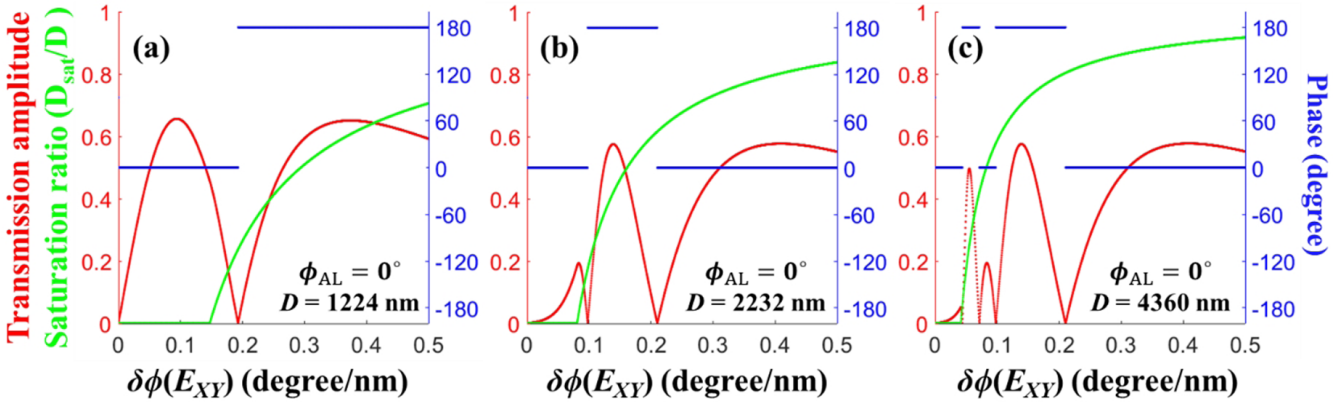

FIG. 5. Transmission amplitudes (red curves) and phases (blue lines) of the transmission coefficients of the BP-C-SLM are simulated as functions of $\delta\phi(E_{XY})$ (in degrees/nm), or equivalently as functions of applied bias voltage. The cell thickness of the BP-C-SLM is D = (a) 1224, (b) 2232, and (c) 4360 nm, with the angle of the alignment layer $\phi_{AL} = 0°$. The phase varies by π when the transmission amplitude crosses zero. All phase values in each plot have been shifted for convenience. The ratios D_{sat} / D of the saturation region's thickness to the total cell thickness are shown as green curves.

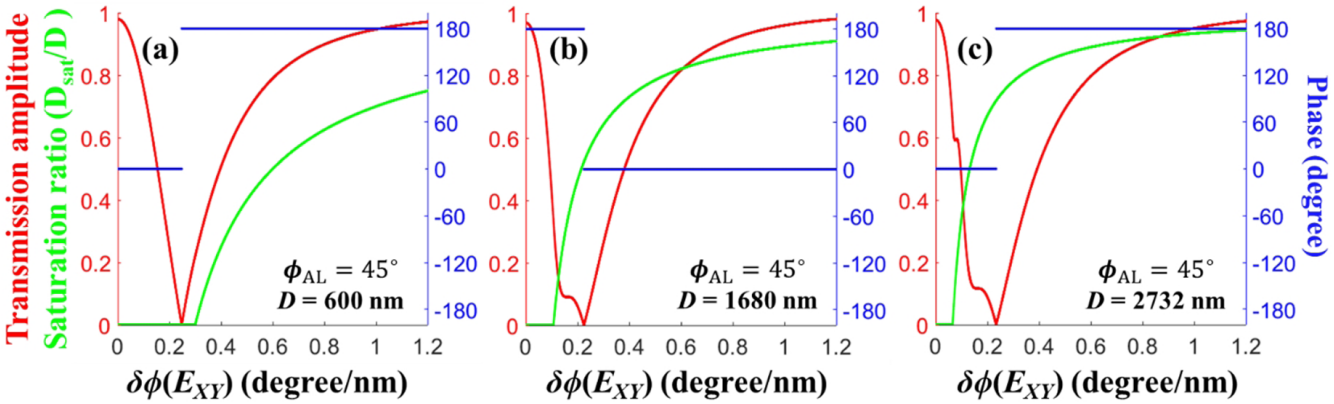

FIG. 6. Amplitudes (red curves) and phases (blue lines) of the transmission coefficients of the BP-C-SLM are simulated as a function of $\delta\phi(E_{XY})$ (in degrees/nm), or equivalently as a function of applied bias voltage. The thickness of the BP-C-SLM is D = (a) 600, (b) 1680, and (c) 2732 nm, with the angle of the alignment layer $\phi_{AL} = 45°$. The phase varies by π when the transmission coefficient crosses zero. All phase values in each plot have been shifted for convenience. The ratios of the saturation region's thickness to the total cell thickness are shown as green curves.

that the amplitude of the transmission coefficient is modulated while the phase is maintained at a constant value for the regions between points at zeroes of the magnitude. The phase difference of the neighboring regions is exactly 180°, as expected from the purely imaginary off-diagonal components of Eq. (9). This suggests that amplitude-only light modulation can be achieved in the constant-phase regions. At the same time, light modulation with a phase difference of 180° can be achieved by dynamically controlling the applied in-plane electric field. This suggests that when the dynamic modulation of $\delta\phi(E_{XY})$ is wide enough, the binary-phase complex light modulation can be achieved across the zeroes in amplitude, as shown in Fig. 5.

The ratios of the saturation region's thickness to the total cell thickness (green curves) are shown in Fig. 5, which clearly indicates that the saturation region becomes wider as the applied bias voltage increases, while there is no saturation region at low bias voltages. With increasing cell thickness, the saturation region becomes wider.

Figure 6 shows the magnitudes (red curves) and phases (blue lines) of the simulated transmission coefficient for the BP-C-SLM with thickness D = 600, 1680, and 2732 nm, and azimuthal angle of the alignment layer $\phi_{AL} = 45°$.

The configuration of the BP-C-SLM with $\phi_{AL} = 45°$does not secure the normally black operation anymore in the off state. However, the perfect black state can be obtained within 0.5 degrees/nm of $\delta\phi(E_{XY})$ with high transmission amplitude, compared to that at $\phi_{AL} = 0°$, by controlling the cell thickness, as shown in Fig. 6.

These simulation results for two representative configurations suggest that BP-C-SLMs can be achieved with both configurations. However, the transmittance of the BP-C-SLM is better with the cell configuration featuring $\phi_{AL} = 45°$, compared to $\phi_{AL} = 0°$, as shown in Figs. 5 and 6. This

suggests that the cell configuration with $\phi_{AL} = 45°$ can be more favorable for the implementation of BP-C-SLMs.

This indicates that the employed configuration can be applied in limited complex spatial light modulators or binary-phase complex spatial light modulators. Thus, these BP-C-SLMs allow one to double the controllability of optical information by an SLM.

V. CONCLUSION

This study describes binary-phase complex spatial light modulators with the specific requirement of mirror symmetry. The proposed structures feature mirror-symmetric distribution of the LC directors with two orthogonal polarizers, and thus control the amplitude information of light as well as the binary phase values. The general approaches developed in this study can be applied to any LC mode or distribution, only with a specific pair that follows the abovementioned required symmetry condition.

Typically, C-SLM structures have been implemented by interconnecting an amplitude SLM (or amplitude-phase coupled SLM) and a phase SLM. The proposed BP-C-SLM structure modulates not only the amplitude of the light but also the binary phase, with a single structure. As a result, the information capacity per pixel of SLMs is doubled.

If a full-range complex SLM is required, the previously developed universal phase-only spatial light modulator (UP-SLM): polarization independently phase controllable SLM [22] is employed with the BP-C-SLM configurations.

Furthermore, this study also suggests that full-range complex spatial light modulators can be achieved when the polar angle of the LC directors is simultaneously manipulated with the azimuthal angle, while the required symmetry conditions are maintained.

The approaches developed in this study will play an important role in promoting the various optical and quantum science applications, such as quantum optics, wave optics, quantum information technology, communication, displays, and holograms.

ACKNOWLEDGMENT

This work was supported by the National Research Foundation of Korea (NRF) grant funded by the Korean government (MSIT) (No. 2019R1F1A106364312, and the BK21 FOUR Program).

REFERENCES

1. W. M. Pimenta, B. Marques, M. A. D. Carvalho, M. R. Barros, J. G. Fonseca, J. Ferraz, M. T. Cunha, and S. Pádua, "Minimal state tomography of spatial qubits using a spatial light modulator," Opt. Express **18**, 24423–24433 (2010).
2. E. J. Fernández, B. Považay, B. Hermann, A. Unterhuber, H. Sattmann, P. M. Prieto, R. Leitgeb, P. Ahnelt, P. Artal, and W. Drexler, "Three-dimensional adaptive optics ultrahigh-resolution optical coherence tomography using a liquid crystal spatial light modulator," Vision Res. **45**, 3432–3444 (2005).
3. J. M. Andersen, S. N. Alperin, A. A. Voitiv, W. G. Holtzmann, J. T. Gopinath, and M. E. Siemens, "Characterizing vortex beams from a spatial light modulator with collinear phase-shifting holography," Appl. Opt. **58**, 404–409 (2019).
4. J. Cho, S. Kim, S. Park, B. Lee, and H. Kim, "DC-free on-axis holographic display using a phase-only spatial light modulator," Opt. Lett. **43**, 3397–3400 (2018).
5. H. Jeong and J. Choi, "Scalable micromesh-digital spatial light modulators," Opt. Express **23**, 26696–26709 (2015).
6. H. Jeong and J. Choi, "Scalable digital spatial light modulator-micromesh heterostructures for real time wave optical applications," Opt. Express **22**, 22865–22881 (2014).
7. K. H. Kagalwala, G. D. Giuseppe, A. F. Abouraddy, and B. E. A. Saleh, "Single-photon three-qubit quantum logic using spatial light modulators," Nat. Commun. **8**, 739 (2017).
8. Z. Qu and I. B. Djordjevic, "Four-dimensionally multiplexed eight-state continuous-variable quantum key distribution over turbulent channels," IEEE Photonics J. **9**, 1–8 (2017).
9. Z. Qu and I. B. Djordjevic, "High-speed free-space optical continuous-variable quantum key distribution enabled by three-dimensional multiplexing," Opt. Express **25**, 7919–7928 (2017).
10. S. Deachapunya, S. Srisuphaphon, P. Panthong, T. Photia, K. Boonkham, and S. Chiangga, "Realization of the single photon Talbot effect with a spatial light modulator," Opt. Express **24**, 20029–20035 (2016).
11. Y. Su, Z. Cai, Q. Liu, L. Shi, F. Zhou, and J. Wu, "Binocular holographic three-dimensional display using a single spatial light modulator and a grating," J. Opt. Soc. Am. A **35**, 1477–1486 (2018).
12. H. Kim, W. Lee, H.-G. Lee, H. Jo, Y. Song, and J. Ahn, "In situ single-atom array synthesis using dynamic holographic optical tweezers," Nat. Commun. **7**, 13317 (2016).
13. Y. Liang, Y. Cai, Z. Wang, M. Lei, Z. Cao, Y. Wang, M. Li, S. Yan, P. R. Bianco, and B. Yao, "Aberration correction in holographic optical tweezers using a high-order optical vortex," Appl. Opt. **57**, 3618–3623 (2018).
14. F. Zhu, S. Huang, W. Shao, J. Zhang, M. Chen, W. Zhang, and J. Zeng, "Free-space optical communication link using perfect vortex beams carrying orbital angular momentum (OAM)," Opt. Commun. **396**, 50–57 (2017).
15. S. Reichelt, R. Häussler, G. Fütterer, N. Leister, H. Kato, N. Usukura, and Y. Kanbayashi, "Full-range, complex spatial light modulator for real-time holography," Opt. Lett. **37**, 1955–1957 (2012).
16. A. J. Macfaden and T. D. Wilkinson, "Characterization, design, and optimization of a two-pass twisted nematic liquid crystal spatial light modulator system for arbitrary complex modulation," J. Opt. Soc. Am. A **34**, 161–170 (2017).
17. Y. Gao, Z. Chen, J. Ding, and H.-T. Wang, "Single ultra-high-definition spatial light modulator enabling highly efficient generation of fully structured vector beams," Appl. Opt. **58**, 6591–6596 (2019).
18. D. A. Gregory, J. C. Kirsch, and E. C. Tam, "Full complex

modulation using liquid-crystal televisions," Appl. Opt. **31**, 163–165 (1992).
19. S. Park, J. Roh, S. Kim, J. Park, H. Kang, J. Hahn, Y. Jeon, S. Park, and H. Kim, "Characteristics of complex light modulation through an amplitude-phase double-layer spatial light modulator," Opt. Express **25**, 3469–3480 (2017).
20. L. Zhu and J. Wang, "Arbitrary manipulation of spatial amplitude and phase using phase-only spatial light modulators," Sci. Rep. **4**, 7441 (2014).
21. L. G. Neto, D. Roberge, and Y. Sheng, "Full-range, continuous, complex modulation by the use of two coupled-mode liquid-crystal televisions," Appl. Opt. **35**, 4567–4576 (1996).
22. M. Choi and J. Choi, "Universal phase-only spatial light modulators," Opt. Express **25**, 22253–22267 (2017).
23. T. D. Wilkinson, D. C. O'Brien, and R. J. Mears, "Dynamic asymmetric binary holograms using a ferroelectric liquid crystal spatial light modulator," Opt. Commun. **109**, 222–226 (1994).
24. J. A. Davis, K. O. Valadéz, and D. M. Cottrell, "Encoding amplitude and phase information onto a binary phase-only spatial light modulator," Appl. Opt. **42**, 2003–2008 (2003).
25. C. Maurer, A. Schwaighofer, A. Jesacher, S. Bernet, and M. Ritsch-Marte, "Suppression of undesired diffraction orders of binary phase holograms," Appl. Opt. **47**, 3994–3998 (2008).
26. W. Chen, "Computer-generated hologram using binary phase with an aperture," Appl. Opt. **56**, 9126–9131 (2017).
27. T. Shimobaba, T. Takahashi, Y. Yamamoto, I. Hoshi, A. Shiraki, T. Kakue, and T. Ito, "Simple complex amplitude encoding of a phase-only hologram using binarized amplitude," J. Opt. **22**, 045703 (2020).
28. P. Yeh and C. Gu, *Optics of Liquid Crystal Displays*, 2nd ed. (John Wiley & Sons, NJ. USA. 2010), Chapter 4.